JACS
JOURNAL OF THE AMERICAN CHEMICAL SOCIETY

Article

pubs.acs.org/JACS

Synergistic Effect in Carbon Coated $LiFePO_4$ for High Yield Spontaneous Grafting of Diazonium Salt. Structural Examination at the Grain Agglomerate Scale

Lénaïc Madec,[†,∥] Donatien Robert,[‡] Philippe Moreau,[†,∥] Pascale Bayle-Guillemaud,[§] Dominique Guyomard,[†,∥] and Joël Gaubicher*[,†,∥]

[†]Institut des Matériaux Jean Rouxel (IMN), Université de Nantes, CNRS, 2 rue de la Houssinière, BP 32229, 44322 Nantes Cedex 03, France

[‡]CEA LITEN, F-38054 Grenoble 9, France

[§]CEA INAC, F-38054 Grenoble 9, France

[∥]Réseau sur le Stockage Electrochimique de l'Energie (RS2E), FR CNRS 3459, France

Supporting Information

ABSTRACT: Molecular grafting of *p*-nitrobenzene diazonium salt at the surface of (Li)$FePO_4$-based materials was thoroughly investigated. The grafting yields obtained by FTIR, XPS, and elemental analysis for core shell $LiFePO_4$−C are found to be much higher than the sum of those associated with either the $LiFePO_4$ core or the carbon shell alone, thereby revealing a synergistic effect. Electrochemical, XRD, and EELS experiments demonstrate that this effect stems from the strong participation of the $LiFePO_4$ core that delivers large amounts of electrons to the carbon substrate at a constant energy, above the Fermi level of the diazonium salt. Correspondingly large multilayer anisotropic structures that are associated with outstanding grafting yields could be observed from TEM experiments. Results therefore constitute strong evidence of a grafting mechanism where homolytic cleavage of the N_2^+ species occurs together with the formation and grafting of radical nitro-aryl intermediates. Although the oxidation and concomitant Li deintercalation of $LiFePO_4$ grains constitute the main driving force of the functionalization reaction, EFTEM EELS mapping shows a striking lack of spatial correlation between grafted grains and oxidized ones.

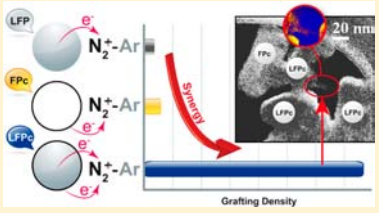

INTRODUCTION

Molecular grafting of surfaces refers to those chemical reactions that allow the functionalization of a substrate (conducting or not) in order to achieve the desired interfacial chemical and physical properties. This field continues to gather momentum and to inspire a growing amount of literature, such as numerous fundamental studies related to reaction mechanisms,[1,2] structure of the organic layer,[3] impact on the bulk properties,[4,5] as well as a plethora of potential applications such as microelectrochemical storage,[6,7] electronics,[8] metal protection against corrosion,[9] and sensors.[10,11] In many cases, strong and durable interactions between the organic layer and the substrate (chemisorption) ($50 < \Delta H < 800$ kJ/mol) are preferred over weak interactions corresponding to physisorption ($\Delta H < 20$ kJ/mol). Chemisorption can result from either noncovalent or covalent bonding. The noncovalent approach has mainly been explored by taking advantage of $\pi-\pi$ interactions between graphene domains and hydrocarbon type functional groups such as phenanthrene, pyrene, and perylene moieties.[10,12] The covalent approach has been achieved through oxidative or reductive mechanisms. Primary and secondary amines have been immobilized on glassy carbon upon electrooxidation.[13] Similarly, carboxylates such as arylacetates,[14,15] as well as hydrazides/hydrazine compounds,[16,17] have been functionalized by anodic polarization on carbon substrates. Reductive pathways have mainly involved the use of vinylic compounds,[18] iodonium[19] and aryldiazonium salts.[20] Recently, interest has been shown in thermal and, more specifically, photolytically induced grafting of aliphatic alkyne[21] and diazirines[22] that are considered very promising approaches in the field of photografting of graphitic carbons. For comprehensive reading on the above chemistry research, the reader is referred to the exhaustive reviews referenced in refs 23−25.

Reductive functionalization with aryldiazonium (ArN_2^+) salt is of particular interest because it can be achieved for a wide variety of substrates such as metals,[26] carbons,[20] and oxides.[27−30] One of the most popular industrial applications of this technique regards the fabrication of inks and pigments by Cabot Corporation[31] since 1993. Although most studies refer to electrochemically induced grafting, spontaneous modification also draws much interest owing to its simplicity and the possibility of using water as the reacting media. As far as electrochemical grafting is involved, it is generally accepted that the underlying mechanism occurs through electron transfer from the substrate to ArN_2^+ together with the cleavage of

Received: May 21, 2013
Published: July 15, 2013

   dx.doi.org/10.1021/ja405087x | J. Am. Chem. Soc. 2013, 135, 11614−11622

dinitrogen. This concerted reaction generates an aryl radical ($Ar^{\bullet}$) that attacks the surface (scheme 1), the efficiency of which resides in its high electrochemical stability. In fact, because $Ar^{\bullet}$ requires a much greater cathodic polarization than the parent ArN_2^+ to be reduced, reduction to the aryl anion, Ar^-, that would be expected to diffuse back into the solution, does not actually occur before the Ar−substrate bond forms. Subsequently, successive attacks of an Ar radical on grafted species lead to the growth of multilayers.

scheme 1:

$$\text{substrate} + 1e^- + ArN_2^+ \rightarrow \text{substrate} + Ar^{\bullet} + N_2$$

$$\text{substrate} + Ar^{\bullet} \rightarrow \text{substrate}-Ar$$

$$\text{substrate}-Ar + Ar^{\bullet} \rightarrow \text{substrate}-Ar-Ar\ldots$$

In the case of spontaneous grafting, however, determination of the functionalization mechanism remains largely controversial. More specifically, either the reaction path can be substrate induced,[1,2,27] in which case $Ar^{\bullet}$ would constitute the main intermediate species (scheme 1), or it can be substrate independent, in which case grafting would occur via an aryl cation (Ar^+) formed by the heterolytic decomposition of ArN_2^+ (scheme 2).[32−34] The latter mechanism which has been proposed in the case of PNBDiaz is promoted by light exposure or by increasing temperatures above 40 °C.[34] In this case, multilayering would arise from the addition of further aryl cations on grafted aromatic rings, coupled by the elimination of protons.

scheme 2:

$$\text{substrate} + ArN_2^+ \rightarrow \text{substrate} + Ar^+ + N_2$$

$$\text{substrate} + Ar^+ \rightarrow \text{substrate}-Ar + H^+$$

$$\text{substrate}-Ar + Ar^+ \rightarrow \text{substrate}-Ar-Ar + H^+$$

Simultaneous involvement of both $Ar^{\bullet}$ and Ar^+ during carbon derivatization by PNBDiaz has also been proposed recently.[35] Alternatively, direct adsorption of the diazonium salt at the surface of gold substrate has been envisioned.[34] In this case, the 5d orbitals of gold are full and can presumably interact with other low-energy, vacant orbitals of the diazonium salt. Fundamental understanding of the mechanism, as well as determination of experimental conditions in which substrate-dependent/-independent pathways prevail, is, however, crucial from the application point of view because one of the main characteristics of the obtained objects relates to the extent and homogeneity of the molecular coverage. If the substrate was the main player in the reaction, then the free enthalpy of the reaction would depend on the ability of the substrate to reduce ArN_2^+. In particular, ΔG would be <0 as long as the Fermi level of the substrate lies above that of the LUMO(ArN_2^+). Whichever the case may be, although spontaneous functionalization of carbon powders is very convenient, literature highlights it is plagued with low grafting yields.[1,25,36] Bélanger and Toupin[1] have proposed that such limitations could be the result of electron transfer from the π system of the carbon that builds positive charges and therefore decreases its Fermi level. As a result, many groups have been searching intensively for new ways to increase the grafting yields,[1,37] especially those in the field of electrochemical storage applications.[37−44]

In this study, we propose a novel strategy for achieving extremely high grafting yields. It is based on a synergistic effect taking place for a core−shell material with an amorphous carbon shell and $LiFe^{II}PO_4$ as the reducing core. $LiFePO_4$ is a well-known material when it comes to lithium battery applications.[45−47] When possessing few defects, $LiFePO_4$ shows a first-order phase transformation on Li delithiation and concomitant oxidation to $Fe^{III}PO_4$.[45,47] This gives rise to a potential plateau in a potential-time representation at nearly +0.15 V vs SCE. By comparison, reduction of *p*-nitrobenzene diazonium salt (referred to as PNBDiaz) on glassy carbon initiates between $0 < U < 0.6$ V (vs SCE) depending on the surface state of the substrate.[48] Therefore, considering the grafting of PNBdiaz at the surface of this type of core−shell material, the $LiFePO_4$ core could thus, in theory, act as an electron reservoir, the capacity of which can be delivered to the carbon surface at an almost constant energy above the Fermi level of PNBDiaz. Our results demonstrate that grafting yields of up to 10 times those typically found in literature[24] can be obtained. The contribution pertaining to each of the core and shell components is described based on an attempt to rationalize underlying physical processes. Meanwhile, the synergistic effect is demonstrated by comparing the corresponding grafting yields with those determined when only one of the two components is active. Furthermore, although the electron reservoir of the $LiFePO_4$ core appears to be the driving force behind achieving such high molecular coverage, thorough examination at the grain agglomerate scale using EFTEM EELS mapping shows that grafted and oxidized core−shell grains are in no way spatially correlated. Finally, this study also serves to shed some light on the reaction mechanisms associated with spontaneous grafting of diazonium salts.

EXPERIMENTAL SECTION

Sample Preparation. Uncoated $LiFe^{II}PO_4$ (referred to as LFP) and carbon-coated $LiFe^{II}PO_4$ (referred to as LFPC) were provided by UMICORE Rechargeable Battery Materials, Belgium. Scanning electron microscopy (SEM) observations of both materials show primary particles with sizes around 150 nm (Figure S7e, Supporting Information). The purity (calc/exp: Li = 4.4/4.3 wt %, Fe = 35.4/34.7 wt %, P = 19.6/17.9 wt % for LFP and Li = 4.3/4.4 wt %, Fe = 34.4/34.4 wt %, P = 19.1/17.6 wt % for LFPC) and carbon content of the LFPC (2.8 wt %) were confirmed by Rietveld analysis (see Figure S1 in the Supporting Information) and elemental analysis (Service Central d'Analyze, CNRS, Vernaison). Molecular grafting of carbon coated $Fe^{III}PO_4$ (referred to as FPC) was also considered. It was obtained by the chemical oxidation of LFPC by NO_2BF_4, which is a strong oxidizing agent (NO_2^+/NO_2 is approximately 5.1 V vs Li^+/Li^0,[49] whereas Fe^{III}/Fe^{II} in $LiFePO_4$ lies at nearly 3.5 V vs Li^+/Li^0). To this purpose, 20 mL of a 1.3 g solution of NO_2BF_4 (1.1 equivalent, Aldrich) in ultrapure acetonitrile (Novolyte) was added drop by drop, in under 5 min, to a 1.5 g LFPC suspension in 40 mL of ultrapure acetonitrile (Novolyte). The mixture was stirred under dry argon for 24 h to complete the reaction:

$$LiFe^{II}PO_4-C + NO_2BF_4 \rightarrow Fe^{III}PO_4-C + LiBF_4 + NO_2 \qquad (1)$$

The sample was subsequently washed by stirring for 30 min in 40 mL of ultrapure acetonitrile under dry argon, followed by sonication in 40 mL of anhydrous acetonitrile for 15 min. The filtered powder was then rinsed with 10 mL of acetone and dried at 60 °C under vacuum for 2 h. The complete reaction (eq 1) was checked by Rietveld refinement of XRD data (Figure S1) leading to the cell parameters a = 9.8263(3) Å, b = 5.7975(2) Å, c = 4.7796(2) Å, V = 272.28(1) Å^3, which are in excellent accordance with published data.[50]

Covalent functionalizations of LFPC, LFP, and FPC were carried out by stirring in a solution of anhydrous acetonitrile containing nitrobenzene diazonium tetrafluoroborate (PNBDiaz, Aldrich). The reaction of PNBDiaz on a carbon surface leads to a grafting of *p*-nitrophenyl groups ($C_6H_4-NO_2$, referred to as PNB) upon departure

dx.doi.org/10.1021/ja405087x | J. Am. Chem. Soc. 2013, 135, 11614−11622

of N_2. Reactions were implemented under a dry argon atmosphere in order to prevent oxidation/hydratation of LFP and LFPC. The covalent functionalization of acetylene black (referred to as Csp) by PNB was performed in water. All grafting reactions were conducted with a ratio of powder mass to solvent volume of 250 mg/16 mL and a reaction duration of 24 h. The theoretical amount L of a dense monolayer coverage of PNB on the surface was estimated by taking the gyration surface area of a grafted phenyl unit (close to 25 $Å^2$ considering van der Waals radii) and specific surface areas of the substrates derived from BET analysis (23 m^2 /g for LFPC and FPC, 8 m^2/g for LFP and 66 m^2/g for Csp). L corresponds to 6.64×10^{-10} mol/cm^2. Accordingly, several samples were prepared with various amounts of PNBDiaz (denoted *n*L): 2L (6×10^{-3} mol/L), 10L (3×10^{-2} mol/L), and 100L (3×10^{-1} mol/L) for LFPC; 10L (3×10^{-2} mol/L) for FPC; 10L (3×10^{-2} mol/L) for LFP; and 2L (6×10^{-3} mol/L) and 10L (3×10^{-2} mol/L) for Csp. Grafted LFPC, FPC, LFP, and Csp will subsequently be referred to as LFPC-NO_2-*n*L (*n* = 2, 10, 100), FPC-NO_2-10L, LFP-NO_2-10L, Csp-NO_2-2L, and Csp-NO_2-10L, respectively. All samples were washed, systematically, first by sonication for 5 min with 250 mL of anhydrous acetonitrile for LFP- and FP-based samples, and with water for Csp, and then three times with 250 mL of anhydrous ethanol in order to remove physisorbed species. However, in order to assess the impact of sonication treatment on the grafting yield, alternative samples were not sonicated; to assess the impact of solvents, a control sample (referred to as LFPC-solvent) was subject to the same procedure as LFPC-NO_2-based samples but without the addition of PNBDiaz. All samples were dried at 60 °C for 10 h prior to physical characterizations.

Elemental Analyses. Analyses were performed by ICP at Service Central d'Analyze−CNRS, Vernaison, France.

Brunauer Emmet Teller (BET). BET surface area analyses were performed with a Micromeritics ASAP 2010 apparatus using nitrogen gas.

Fourier Transform Infrared (FTIR) Spectroscopy. FTIR spectra were collected with a Bruker Vertex 70 in absorbance mode using KBr pellets and a DTGS detector at a resolution of 4 cm^{-1}. Pellets were made from a mixture of 1 mg of sample powder and 300 mg of KBr.

X-ray Photoelectron Spectroscopy (XPS). XPS was performed with a Kratos Axis Ultra spectrometer using an Al Kα monochromatic beam working at 1486.6 eV. Data were collected at room temperature, and the operating pressure in the analysis chamber was kept below 8×10^{-9} Torr. Powders were deposited onto stainless steel holders and all core spectra were recorded in the CAE (constant analyzer energy) mode with an analyzer pass energy of 20 eV. Data treatment was performed using CasaXPS software. In order to determine atomic concentrations (in mol %), the pseudo-Voigt functions common to each element, constrained by full width at half-maximum (fwhm) ranges, were used and all spectra were calibrated taking 284.5 eV (graphitic like carbon) as a reference binding energy.

XRD and Rietveld Analysis. Polycrystalline samples were analyzed by X-ray diffraction, using an X-Pert Panalytical diffractometer, equipped with Cu K$\alpha_{1,}\alpha_2$ radiation (λ_1 = 1.540598, λ_2 = 1.544394, R = 0.4969, potential V = 45 kV, intensity I = 35 mA), and with a monochromator eliminating Kβ radiation. The analyses were carried out using a $\theta-\theta$ configuration, with 2θ angle steps of 0.017 from 15° to 85° and counting times of 38 s per step. Rietveld analyses were achieved by using the FullprofSuite package[51] software in a *Pnma* metrics for all phases. Refinement was conducted starting from the atomic positions published by Yamada et al.,[50] using a linear background and spherical harmonics for the line shape description. Peak fitting of the (200) line was conducted using a pseudo-Voigt function implemented in Winplotr.[52]

Electrochemical Tests. For this purpose, an electrode of 25 mg was prepared from a self-supported film constituted of 95 wt % of LFPC and 5 wt % of PTFE. Powders were hand-mixed and pressed on a stainless grid at 5 tons. The electrolyte (LP30) obtained from Novolyte as a high-purity grade is 1 M $LiPF_6$ in 1:1 EC-DMC and was used as received. Karl Fischer titration indicates that LP30 contains approximately 10 ppm of H_2O. The open-circuit-potential (OCP) was monitored at 22 °C by a potentiostat (VMP-Biologic SA, Claix, France) using EC-Lab software (Biologic SA, version 10.18), a three-electrode cell with Li^0 as the reference electrode, and a stainless grid as the counter electrode. Potentials are reported vs Li^+/Li^0.

Upon OCP measurement, the electrode was washed with LP30 and transferred into a new cell for Li intercalation. Li intercalation was performed at 22 °C in galvanostatic mode using a current equivalent to intercalation of 1Li in 25 h down to 3 V vs Li^+/Li^0. The potential was maintained at this level until the current reached a pseudoequilibrium corresponding to 0.01 Li/h.

TEM-EELS Experiments. These experiments were performed on a FEI-Titan microscope with a probe corrector and a GIF spectrometer. In order to avoid radiation damage of the grafted molecules, measurements were made at liquid nitrogen temperature at 100 kV. EELS spectra were obtained in energy filtered mode (EFTEM). Series of EFTEM images with an energy selecting slit of 1 eV (from −3.5 to 29.5 eV) were acquired in order to fill the so-called data cube (x,y,ΔE), where ΔE was the electron energy loss, and x and y denoted the position in the image. The EELS spectra were reconstructed from these stacks of EFTEM images using the Digital Micrograph module "Spectrum Imaging". Mapping at the L_{23} threshold of Fe, and the K threshold of O and N, was achieved by recording three filtered images (two for the pre-edge and one postedge[53]).

RESULTS

Evidence and Structural Impact of Molecular Grafting. Figure 1 shows the FTIR spectra of LFPC-NO_2-*n*L

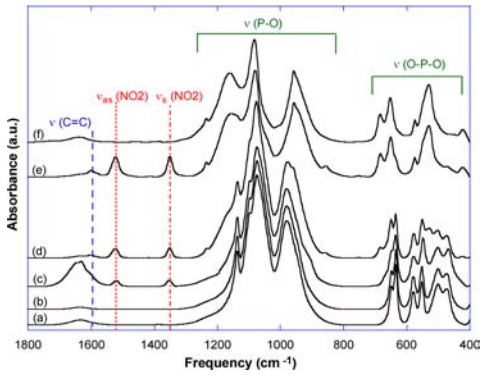

Figure 1. FTIR spectra of (a) pristine LFPC, (b) LFPC-solvent, (c) LFPC-NO_2-2L, (d) LFPC-NO_2-10L, (e) LFPC-NO_2-100L, and (f) pristine FPC.

samples. With regard to the LFPC-solvent (Figure 1b), no significant change is detected in the region of 1800−1250 cm^{-1} when compared to pristine LFPC (Figure 1a), whereas for LFPC-NO_2-*n*L, antisymmetric and symmetric vibration bands assigned to NO_2 groups[26] are detected at 1520 and 1350 cm^{-1} respectively. Corresponding intensities increase with *n*L from 2L to 100L. The frequency difference between the antisymmetric and symmetric vibrations equals nearly 170 cm^{-1} which is in the range reported for solids[54] (159−177 cm^{-1}) in accordance with the confinement of NO_2 groups to the carbon surface. In addition, the vibration band of the C=C bonds associated with the aromatic ring appears at 1600 cm^{-1}. However, the stretching vibration band of the N_2^+ diazonium group (2300−2150 cm^{-1}) present in PNBDiaz is never observed, regardless of the value of nL. Therefore, the signals ascribed to NO_2 groups and aromatic rings correspond to diazonium salts that have reacted. Given the use of ultrasonic washing, FTIR results comply with strong interactions between the carbon shell and organic species. Vibration bands in the regions of 1300−800 and 800−400 cm^{-1} that correspond to elongation and deformation of phosphate PO_4^{3-} anions,

dx.doi.org/10.1021/ja405087x | J. Am. Chem. Soc. 2013, 135, 11614−11622

respectively, are particularly useful for monitoring the iron redox state of the LFPC core. In regard to the LFPC-solvent (Figure 1b), no significant change is observed for these bands. For LFPC-NO_2-2L (Figure 1c), however, very slight intensity variations can be observed in the 1300−800 cm^{-1} region. These modifications grow progressively as n increases. In fact, with respect to the LFPC-NO_2-10L (Figure 1d), not only are further changes in the intensity detected, but also changes in the position of the peaks in the 1300−800 cm^{-1} and 800 to 400 cm^{-1} regions. These results suggest that oxidation of LFPC took place during the reaction with PNBDiaz. These modifications are even more pronounced for the sample LFPC-NO_2-100L (Figure 1e), where vibration bands of PO_4^{3-} anions are similar to those observed for $Fe^{III}PO_4$ (Figure 1f), implying a near-to-total oxidation of LFPC upon reaction with large amount of PNBDiaz. It should be noted that very similar results for both LFPC-NO_2-10L and LFPC-NO_2-100L were observed if sonication treatments were not conducted during sample preparation (see Figure S2).

Interestingly, FTIR spectra of the LFP-NO_2-10L and FPC-NO_2-10L samples (Figure 2b and c) do not show characteristic

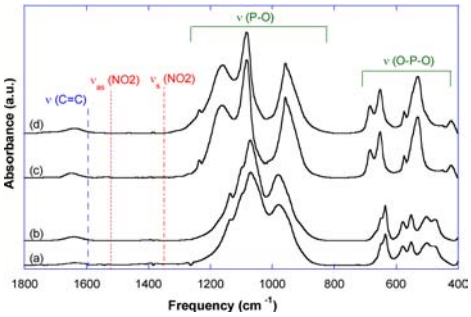

Figure 2. FTIR spectra of (a) pristine LFP, (b) LFP-NO_2-10L, (c) FPC-NO_2-10L, and (d) pristine FPC.

vibration bands of NO_2 and $C{=}C_{aromatic}$ groups in the 1550−1300 and 1650−1500 cm^{-1} regions, respectively. With respect to LFP-NO_2-10L (Figure 2b), no change of PO_4^{3-} vibration bands could be detected in the 1300−800 and 800−400 cm^{-1} regions, suggesting that if a reaction with PNBDiaz occurred (see further down), it was very limited.

The redox state of the $LiFePO_4$ core was monitored during functionalization by in situ measurement of the open-circuit potential (OCP). Downard et al.[35] measured a ∼300 mV sharp, initial increase of the OCP of a carbon electrode after the addition of PNBDiaz salt in water or acetonitrile solutions. This OCP increase was followed by decay back to the initial value in water, and by ∼100 mV in acetonitrile. This behavior was ascribed to depolarization of the carbon surface upon proton removal. In this study, however, observations differed. After 5 min of equilibration in LP30, the OCP was nearly constant, close to 3.25 V vs Li^+/Li^0 (Figure 3). At this point, a LP30 solution of PNBDiaz (3×10^{-2} mol/L) was introduced into the electrochemical cell. The addition of PNBDiaz induced a jump of 40 mV followed by a smooth increase of the potential up to 3.44 V over five hours. The potential then remained locked at this value for 17 additional hours since no potential decrease was observed, as in reference.[35] This potential corresponds to the first-order phase transformation of $Li_{1-\delta}FePO_4/Li_\gamma FePO_4$ (δ = 0.05 and γ = 0.11 as reported in ref 50) that is encountered during near-to-equilibrium Li deintercalation from $LiFePO_4$. The electrode was subsequently rinsed with LP30 and

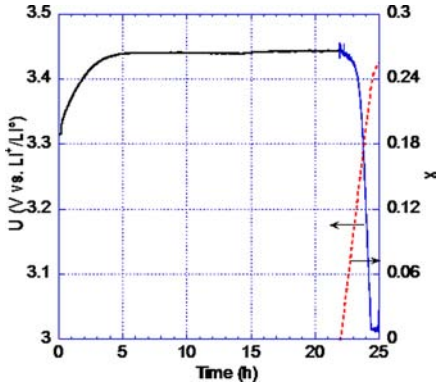

Figure 3. OCP variation of LFPC during reaction with PNBDiaz in LP30 electrolyte, followed by Li insertion down to 3 V along with corresponding variation of x (mol of e^-/Li^+ per mol $LiFePO_4$ initially contained in the electrode).

transferred into a new cell with LP30 and Li^0 as the electrolyte and negative electrode, respectively. The initial potential was nearly unchanged compared to that measured prior to cell transfer. Discharge was conducted down to 3 V vs. Li^+/Li^0. As shown in Figure 3, close to 0.25 mol of e^-/Li^+ per mol of the $LiFePO_4$ initially contained in the electrode (x = 0.25 in Figure 3) could be reinserted, which serves to underline the fact that redox behavior of the LFP core during functionalization by PNBDiaz is correlated to Li deintercalation.

Rietveld analysis of XRD diagrams related to the LFPC-NO_2-nL (n = 10 and 100) were conducted in order to get a more accurate description of these findings. The corresponding refinement procedure, as well as observed, calculated, and differential curves, are reported in Figure 4a and in Figure S1, along with reliability factors, cell parameters, and respective mass fraction in Table S1. All samples, including the LFPC, LFPC-solvent, and FPC standards, were refined to the ideal atomic structure in a *Pnma* metric, in excellent agreement with previous reports.[50] As illustrated in Figure 4a for LFPC-NO_2-10L, grafting of PNBDiaz starts off with the appearance of the $Li_\gamma FePO_4$ ($V \sim 274$ Å^3) and $Li_{1-\delta}FePO_4$ ($V \sim 290$ Å^3) phases which are known to form upon Li/e- removal from $LiFePO_4$.[50] Rietveld analysis indicates 73 wt % (72 mol %) and 27 wt % (28 mol %) for $Li_{1-\delta}FePO_4$ and $Li_\gamma FePO_4$, respectively. Assuming that δ = 0.05 and γ = 0.11 as reported in reference,[50] Li intercalation into sample LFPC-NO_2-10L should lead, in theory, to x = 0.29 which would be in very good agreement with the x = 0.25 determined from Figure 3. As regards the LFPC-NO_2-2L and LFP-NO_2-10L, the proportion of $Li_\gamma FePO_4$ was too low to be sufficiently refined by Rietveld analysis. Accordingly, since the LFPC and FPC have very close F_{hkl} factors, the weight percent (wt %) of the two phases was evaluated from integration of line intensity for a given (hkl) set. This analysis was conducted for the (200) line, since it shows the highest angular resolution between the two phases. The corresponding fits are those reported in Figure S3, while estimated wt % values are provided in Table S1. A comparison of the wt % obtained for LFPC-NO_2-nL (n = 2, 10 and 100) and LFP-NO_2-10L is shown in Figure 4b. It is clear from (i) in the LFPC-NO_2-nL series, that the $Li_\gamma FePO_4$ phase grows at the expense of the $Li_{1-\delta}FePO_4$ one, and (ii) that LFP-NO_2-10L contains much less of the $Li_\gamma FePO_4$ phase (2 wt %) than do LFPC-NO_2-2L (5 wt %) and LFPC-NO_2-10L (27 wt %). The

dx.doi.org/10.1021/ja405087x | J. Am. Chem. Soc. 2013, 135, 11614−11622

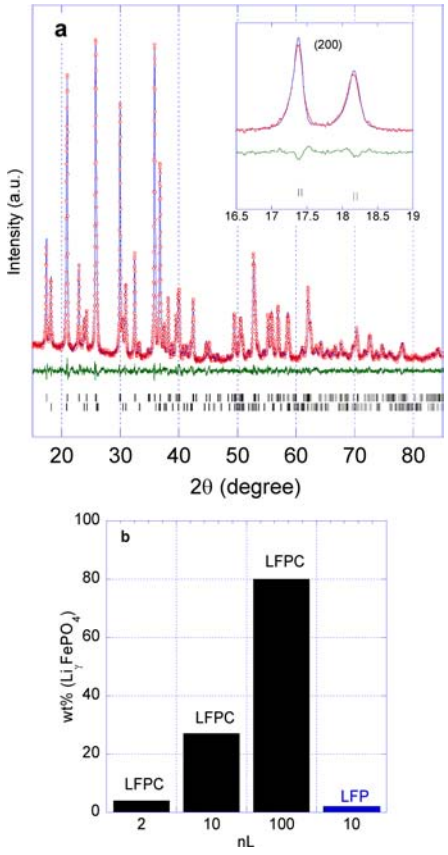

Figure 4. Observed, calculated, and differential curves (plotted on the same scale), as well as Bragg positions obtained upon Rietveld refinement for (a) LFPC-NO_2-10L (a close up of the (200) line of $Li_{1-\delta}FePO_4$ and $Li_\gamma FePO_4$ phases is provided in the inset), and (b) weight proportion of $Li_\gamma FePO_4$ derived from Rietveld analysis of LFPC-NO_2-*n*L and LFP-NO_2-10L diagrams.

next section presents a comparison of the redox state of grafted samples to their molecular coverage.

Determination of Molecular Coverage. Molecular coverage of PNB (referred to as Γ_{chem}) on the carbon shell of LFPC-NO_2-*n*L and FPC-NO_2-10L, and on the surface of LFP-NO_2-10L, was determined by coupling elemental analyses and XPS results. The true reactivity of the surface toward molecular grafting is reflected by Γ_{chem} values in mol/cm^2. The surface areas available for grafting reactions were therefore evaluated from BET analysis (see Experimental Section), whereas the amount of PNB was derived from the atomic ratio N_{NO_2}/N_{total} obtained from XPS semiquantitative analysis (Figure S4), multiplied by the wt % of N_{total} acquired from elemental analysis. Corresponding values of Γ_{chem} are reported in Table 1 and in Figure 5. In the case of LFPC-NO_2-*n*L, the spontaneous grafting of the carbon substrate increases with *n*L up to an extremely high value of $\Gamma_{chem} = 60 \times 10^{-10}$ mol/cm^2 (14.4 wt %) for $n = 100$.

According to the XRD results (Figure 4b), LFPC-NO_2-100L is composed of 20 wt % (20 mol %) of $Li_{1-\delta}FePO_4$ and 80 wt % (80 mol %) of $Li_\gamma FePO_4$. Assuming $\delta = 0.05$ and $\gamma = 0.11$, as reported in ref 50, the associated amount of electrons that were consumed starting from LFPC is 0.72/mol$_{LFPC}$. Therefore, considering that all these electrons are associated with molecular grafting reactions according to the stoichiometry (1 mol of e^- provided by LFPC corresponds to the grafting of 1 mol of PNBDiaz), the theoretical grafting yield should be 207 $\times 10^{-10}$ mol/cm^2. This result shows that only 29% of available electrons are efficiently used for PNBDiaz grafting. We note that this value is in the same range (25%) for LFPC-NO_2-10L. As would be expected, it appears that a portion of the electrons provided by LFPC, are consumed by side reactions,[38] and/or that sample washing using sonication, as described in the Experimental Section, could induce a partial cleavage of the grafted organic layer. We therefore evaluated samples prepared under identical conditions, but without sonication washing. Results reported in Table S2 clearly demonstrate that sonication does not significantly modify (less than 3%) the grafting yields.

Table 1. Semiquantitative XPS Analysis, Elemental Analysis, and Γ_{chem} for LFPC-NO_2-*n*L, FPC-NO_2-10L, LFP-NO_2-10L, and Csp-NO_2-*n*L Samples

substrate	*n*L	N_{NO_2}/N_{total} (XPS)[a]	N_{total} (wt %) (El-Ana)[a]	Γ_{chem} (wt %)[a]	$\Gamma_{chem} \times 10^{10}$ (mol/cm^2)[a]
LFPC	0	0	0	0	0
LFPC	2	0.49	0.51	2.2	7.9
LFPC	10	0.61	0.77	4.1	15.2
LFPC	100	0.56	2.95	14.4	60.0
FPC	10	0.17	0.30	0.4	1.6
LFP	10	0.10	0.14	0.1	0.4
Csp	2	0.72	0.65	4.08	5.1
Csp	10	0.68	0.7	4.14	5.2

[a]Experimental errors are less than 5% upon repeating the grafting, XPS, and elemental analyses.

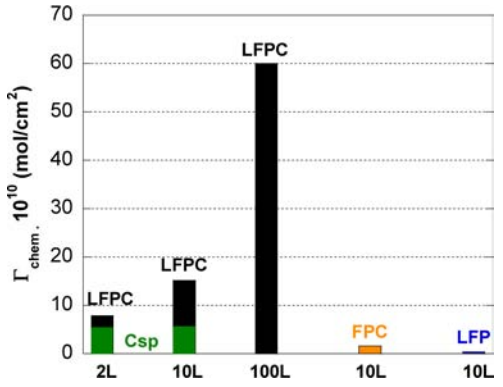

Figure 5. Comparison of Γ_{chem} measured for LFPC-NO_2-*n*L, LFP-NO_2-10L, FPC, and Csp-NO_2-*n*L samples.

Although most values for spontaneous grafting of diazonium salts on carbon substrate reported in literature are restrained to a few 10^{-10} mol/cm^2, caution should be exercised when comparing our results as the grafting yield may depend on experimental conditions, as well as the nature of the carbon substrate (usually carbon blacks with different degree of graphitization). The surface of the LFPC carbon coating is known to contain many more sp^3 defects and oxygenated functionalities than most carbons used in studies related to spontaneous grafting of PNBDiaz.[23−25] Bélanger et al. have demonstrated that the grafting yield of carbon surface is not significantly influenced, even upon strong oxidation using nitric acid reflux. However, in order to facilitate a more direct comparison of our results with those from literature, PNBDiaz grafting of the Csp acetylene black sample and grafting yield determination were conducted using our experimental conditions (Figure S5 and S6). As shown in Table 1 and

dx.doi.org/10.1021/ja405087x | J. Am. Chem. Soc. 2013, 135, 11614−11622

Figure 5, values obtained for Csp-NO_2-nL (n = 2 and 10) are significantly lower than those obtained for LFPC-NO_2-2L. We note that a similar grafting yield was obtained for n = 2 in the case of more heavily graphitized carbon black using very similar experimental conditions.[5] Moreover, with respect to the Fe(III) containing FPC-NO_2-10L, $\Gamma_{chem} = 1.6 \times 10^{-10}$ mol/cm^2, which is close to 10 times lower than for LFPC-NO_2-10L. This illustrates the decisive role of the $LiFePO_4$ core component of LFPC in regard to the extent of the grafting yield. On the other hand, if the $LiFePO_4$ core is not covered by a carbon shell, as with the LFP-NO_2-10L, then $\Gamma_{chem} = 0.4 \times 10^{-10}$ mol/cm^2, which is nearly 40 times less than LFPC-NO_2-10L. Accordingly, the grafting yield of the $LiFePO_4$-core/C-shell (LFPC) composite is larger than the sum of that obtained for $LiFePO_4$-core alone (LFP), added to that of the FPC sample where only the C-shell can provide electrons. This demonstrates the significant synergistic effect that stems from the use of a $LiFePO_4$−C carbon-shell composite.

Grafting Mechanism and Local Examination. These results indicate that the grafting mechanism of LFPC is driven by the reducing power of the $LiFePO_4$ core, for which the oxidation is compensated by Li deinsertion. Correspondingly, formal grafting mechanisms can be proposed which neglect the contribution of the carbon shell. They are divided in three groups depending on the number of mol of grafted PNB (referred to as y) vs the Li composition range x of the core: if $y < 0.05$, Li_xFePO_4 is in a solid solution composition range and the amount of grafted PNB depends on x (eq 2); if $0.05 < y < 0.11$, $Li_{0.05}FePO_4$ forms all along the biphasic domain together with $Li_{0.11}FePO_4$, so that the amount of grafted PNB depends on the molar fraction of the these two phases (eq 3); and, last, if $0.11 < y$, Li_xFePO_4 is in a second solid solution composition range (eq 4). Therefore, the three corresponding groups of formal reactions are as follows:

$$\begin{aligned} &LiFe^{II}PO_4{-}C + x(C_6H_4NO_2)N_2^+BF_4^- \\ &\rightarrow Li_{1-x}Fe_x^{III}Fe_{1-x}^{II}PO_4{-}C{-}(C_6H_4NO_2)_x + xLiBF_4 \\ &\quad + xN_2 \end{aligned} \tag{2}$$

$$\begin{aligned} &LiFe^{II}PO_4{-}C + (0.05 + 0.84n)(C_6H_4NO_2)N_2^+BF_4^- \\ &\rightarrow (1 - n)Li_{0.95}Fe_{0.05}^{III}Fe_{0.95}^{II}PO_4{-}C{-} \\ &\quad (C_6H_4NO_2)_{0.05} + nLi_{0.11}Fe_{0.89}^{III}Fe_{0.11}^{II}PO_4{-}C{-} \\ &\quad (C_6H_4NO_2)_{0.89} + (0.05 + 0.84n)LiBF_4 \\ &\quad + (0.05 + 0.84n)N_2 \end{aligned} \tag{3}$$

$$\begin{aligned} &LiFe^{II}PO_4{-}C + (0.89 + x)(C_6H_4NO_2)N_2^+BF_4^- \\ &\rightarrow Li_{0.11-x}Fe_{0.89+x}^{III}Fe_{0.11-x}^{II}PO_4{-}C{-} \\ &\quad (C_6H_4NO_2)_{0.89+x} + (0.89 + x)LiBF_4 \\ &\quad + (0.89 + x)N_2 \end{aligned} \tag{4}$$

Local examination of grafted samples was conducted for LFPC-NO_2-10L and LFPC-NO_2-2L using TEM and EELS experiments. In these experiments, most of the particles studied are smaller than 100 nm in order to facilitate EELS analysis. Dispersion in particle sizes in fact exists in the pristine sample (50−200 nm) as shown in SEM images (Figure S7e). Figure 6a shows a typical image of LFPC-NO_2-10L (that of LFPC-NO_2-2L is provided in Figure S7c). As opposed to pristine LFPC and LFPC-solvent (Figure S7a,b), the occurrence of an amorphous layer (with a characteristic contrast found in the case of polymers) ascribed to the organic compound is clearly observed for grafted samples (marked by full arrows in Figure 6a and S7c,d), thus confirming the grafting of PNB. However, thorough examination of the LFPC-NO_2-10L sample shows that organics are not homogeneously deposited at the surface, since some grains do not appear to be grafted (dashed arrows).

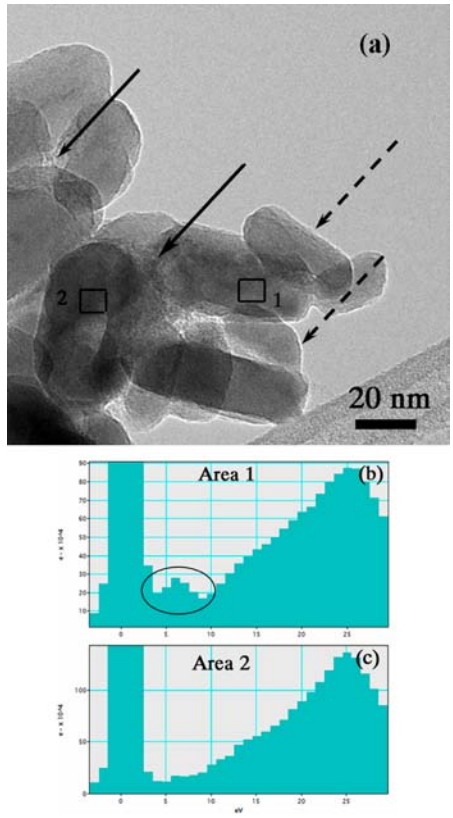

Figure 6. (a) TEM image of LFPC-NO_2-10L, (b) reconstructed EELS spectrum corresponding to region 1, and (c) reconstructed EELS spectrum corresponding to region 2.

EELS spectra that have been built from EFTEM series corresponding to regions 1 and 2 are shown in Figure 6b and c. The occurrence of a peak at 6 eV in region 1 is characteristic of the $Fe^{III}PO_4$[53,55] phase, therefore confirming the oxidation of $LiFePO_4$ upon grafting. Furthermore, as expected for the 10L stoichiometry, the grafting reaction is not complete and other regions, such as region 2, are still in the $LiFePO_4$ state. In Figure 7, another region of the LFPC-NO_2-10L sample is presented. The circled area outlines a ∼40 nm molecular junction that bridges two neighboring grains. As inferred from Figure 7b, this junction gradually vanishes under the electron beam. Furthermore, the iron signal is absent from the bridge (Figure S8). This is the first time, to our knowledge, that the ability of diazonium chemistry to build such a large and anisotropic structure for the spontaneous grafting of carbon-based powder substrates has been evidenced. As per the occurrence of azo bridges suggested by XPS results (see Figure S4), this structure results from multilayer stacking of PNBDiaz. As was mentioned in the introduction section, it is still debatable as to which of several grafting mechanisms are responsible for spontaneous reactions. Two main reaction pathways have thus far been envisaged: homolytic or heterolytic dediazoniation with the occurrence of an intermediate aryl

dx.doi.org/10.1021/ja405087x | J. Am. Chem. Soc. 2013, 135, 11614−11622

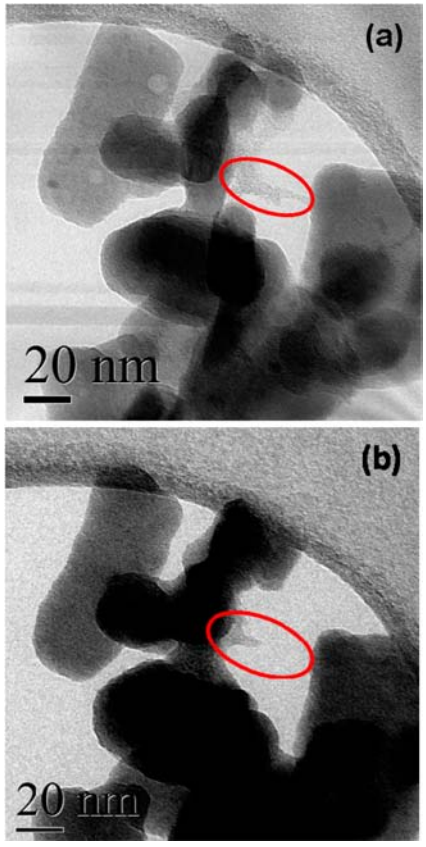

Figure 7. (a) TEM bright field images of LFPC-NO_2-10L crystals. The circled region highlights a molecular bridge formed by the stacking of PNB between two neighboring grains (a) before and (b) after electron beam damage.

radical or aryl cation, respectively (see Introduction, scheme 1 and 2). Downard et al. showed that the overall grafting mechanism of carbon substrate is, in fact, the sum of both scheme 1 and 2, but with the former being predominant and faster.[35] We note that since acetonitrile and aqueous acid solutions have relatively low nucleophilicity parameters, reduction of PNBDiaz by the solvent in order to generate aryl radicals is not expected to be a major dediazoniation pathway; instead, thermal- or light-assisted decomposition of PNBDiaz leading to the formation of aryl cations is a more likely candidate.[56] However, radical cations have very short lifespan and therefore only those formed near the surface can graft. This substrate-independent path would, however, lead to comparable grafting yields for both LFPC and FPC. Thus, in our case, the aryl cation-based mechanism can be regarded as occurring in the background. As noted, Pinson and Andrieux showed that an Ar^- anion can form and diffuse back into the solution.[57] Since the formation of these Ar^- anions were shown to be restricted to a very high driving force, and considering that the inner potential is lower than 450 mV [the LUMO(PNBDiaz) is situated at 0.6 V vs. SCE and the Fermi level of LFP at 0.15 V vs. SCE], the latter mechanism is unlikely.

Because the resulting surface coverage of LFP grains is highly inhomogeneous, it seemed an interesting idea to study the degree of spatial correlation between oxidized and grafted areas. To this end, EFTEM EELS mapping of LFPC-NO_2-10L was attempted. This technique was recently reported by some of us as being a very efficient and swift method for discriminating between $LiFePO_4$ and $FePO_4$ crystals[53] among a vast array. EFTEM/EELS maps have been built taking into account the ratio of the energy losses between 4.5 and 6.5 eV and those at higher energy to reduce thickness effects.[55] A typical image is shown in Figure 8, where orange crystals are characteristic of a phase of composition close to $FePO_4$, and purple ones of a composition close to $LiFePO_4$.

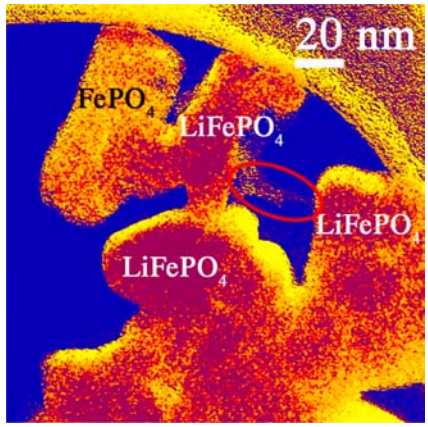

Figure 8. EFTEM EELS mapping of LFPC-NO_2-10L shown in Figure 7. Purple crystals correspond to a phase of composition close to $LiFePO_4$ while orange ones correspond to a phase of composition close to $FePO_4$. Edges of crystals sometimes appear orange due to extreme surface plasmon effects, as well as at the carbon coating.

We were unable to find any crystals that contained both the $FePO_4$ and $LiFePO_4$ phases, thereby confirming the domino-cascade mechanism proposed by Delmas and Croguenec.[58] This mechanism is characterized by the fact that during Li/e-removal from $LiFePO_4$, the growth of $FePO_4$ domains is much faster than its nucleation, in such a way that Li deintercalation proceeds as a wave moving through the entire crystal. In the case at hand, however, it is very surprising that LFPC crystals appear on both sides of the molecular bridge while, on the contrary, the oxidized FPC grain is not functionalized. This striking feature was encountered in many parts of the sample. As shown previously, results indicate that spontaneous grafting of LFPC mainly takes place via a substrate-assisted reduction of PNBDiaz. The LFPC grains constitute an electron reservoir that acts as an inner electron source. This reaction path is consistent with the observation of large, multilayer structures (Figures 6a and 7) that have only been reported, as far as carbon substrates are concerned, in the case of electrochemical grafting of diazonium salts.[23] As documented in the Introduction, it has been proposed that such reactions may take place via intermediate $Ar^\bullet$ species. These $Ar^\bullet$ species would result from concerted homolytic dediazoniation in the vicinity of the surface, and couple immediately with the substrate. It is therefore rather counterintuitive that some grains are oxidized and not grafted, whereas others are grafted but not oxidized. At least two hypotheses can be offered in order to explain this result. At the grain agglomerate scale, the carbon coating is seen by electrons as continuous (either because the carbon shell of neighboring grains have merged during the synthesis procedure, or because activation barriers at physical contacts between LFPC grains enable facile hopping at room temperature). A low electronic activation barrier between primary particles of LFPC clusters has recently been confirmed by broadband dielectric spectroscopy measurements of LFPC

dx.doi.org/10.1021/ja405087x | J. Am. Chem. Soc. 2013, 135, 11614−11622

samples.[59] On this basis, once Li deintercalation has been initiated for a specific grain, the propagation of the deintercalation wave via the domino-cascade process enables fast removal of huge amounts of electrons that are available to react with aryl radical species at the surface of the whole cluster. Correspondingly, massive grafting is expected to take place where energy barriers for the C−C bond formation are the lowest (defects, edges, etc.). Alternatively, a second mechanism might involve the $Ar^{\bullet}$ species that would form at the surface of a specific grain, and then diffuse away from these sites to react at the surface of other grains. In the present case, given the strong participation of the substrate in the grafting extent, highly reactive $Ar^{\bullet}$ species are thought to react quasi instantaneously at the surface of the carbon substrate. We believe this second mechanism is less likely than the domino-cascade assisted one.

The above considerations serve to demonstrate that the use of this reducing core−shell material coupled with EFTEM EELS mapping enables the localization of both the electron source and the grafting spots. This type of "labeling" opens up new possibilities for achieving a deeper insight into diazonium salt chemistry. Moreover, as far as Li battery application is concerned, the possibility of discriminating the e^- withdrawal spots (where grafting occurs) from Li^+ removal ones ($FePO_4$ type grains), might help in understanding which factor makes some grains more prone to Li deintercalation than others within a cluster of primary particles. Such issues are of great importance in the search for improved power response and cycle life.[60] Indeed, within a composite electrode, the more reactive grains "work" more than the other grains, and are therefore expected to be responsible for storage failures appearing during extended cycling. In this regard, the precession electron diffraction technique was used to characterize the composition of a large number of particles with a nanometer resolution, both at the grain and agglomerate scales.[53] It was pointed out that, for partially delithiated electrodes, $FePO_4$ grains are larger than $LiFePO_4$ ones and that a core shell model or spinodal decomposition can be envisaged at the agglomerate scale. Furthermore, it has been shown that under high current load, a spatial inhomogeneity of composition occurs at the electrode scale, some grains or agglomerates of grains being preferentially involved in the electrochemical reaction.[61,62] In our case, molecular anchoring enables to determine where electrons have been removed from agglomerates, which, in a way, mimics the electronic contacts with the carbon percolating network of the composite. In situ grafting of PNB in ionic liquid media is currently evaluated using EFTEM.

CONCLUSION

Molecular grafting of *p*-nitrobenzene diazonium salt on the surface of a core−shell composite of carbon-coated $LiFePO_4$ was examined and compared to that of core−shell carbon-coated $FePO_4$, as well as uncoated $LiFePO_4$. Results highlight a synergistic effect occurring from the simultaneous contribution of both the carbon shell and the reducing $LiFePO_4$ core. The core $LiFePO_4$ constitutes an electron reservoir, from which most of the capacity can be delivered at a constant energy above the LUMO of the diazonium derivative. However, the existence of the carbon shell appears to be mandatory with respect to triggering a highly effective reaction. This synergy enables unprecedentedly high grafting yields from simple spontaneous grafting at the surface of the amorphous carbon substrate. Accordingly, results clearly point to a spontaneous grafting mechanism associated with a strong participation of the substrate, which agrees with the occurrence of an intermediate radical species.

Although the oxidation and concomitant Li deintercalation of $LiFePO_4$ grains constitutes the driving force of the functionalization reaction, EFTEM EELS mapping revealed a striking lack of spatial correlation between grafted grains and oxidized ones. Accordingly, it appears that within a grain cluster, a certain trait of LFP grains might tend to favor the Li deintercalation of particular grains.

These results and, more particularly, the labeling of both grain redox reactivity and grafting reactivity as inferred from EFTEM EELS mapping should serve to optimize as well as boost comprehension of spontaneous functionalization processes involving diazonium salts. This seems especially relevant when considering the fact that very high grafting yields can readily be obtained, which is a deciding factor for many applications such as electrochemical energy storage. It also paves the way for a deeper understanding of the redox reactivity of $LiFePO_4$ grains at the cluster scale, which is vital to the power response and cycle life of Li battery devices.

ASSOCIATED CONTENT

Supporting Information

Additional Rietveld and line analysis as well as complementary elemental analysis, FTIR, XPS, TEM, and EFTEM EELS data. This material is available free of charge via the Internet at http://pubs.acs.org.

AUTHOR INFORMATION

Corresponding Author

joel.gaubicher@cnrs-imn.fr

Notes

The authors declare no competing financial interest.

ACKNOWLEDGMENTS

The authors are grateful to Umicore for having provided LFP and LFPC samples.

REFERENCES

(1) Toupin, M.; Bélanger, D. *Langmuir* **2008**, *24*, 1910−1917.
(2) Le Floch, F.; Simonato, J.-P.; Bidan, G. *Electrochim. Acta* **2009**, *54*, 3078−3085.
(3) Brooksby, P. A.; Downard, A. J. *Langmuir* **2004**, *20*, 5038−5045.
(4) Saab, A. P.; Garzon, F. H.; Zawodzinski, T. A. *J. Electrochem. Soc.* **2003**, *150*, A214−A218.
(5) Madec, L.; Humbert, B.; Lestriez, B.; Brousse, T.; Cougnon, C.; Guyomard, D.; Gaubicher, J. *J. Power Sources* **2013**, *232*, 246−253.
(6) Pech, D.; Guay, D.; Brousse, T.; Bélanger, D. *Electrochem. Solid-State Lett.* **2008**, *11*, A202−A205.
(7) Madec, L.; Bouvrée, A.; Blanchard, P.; Cougnon, C.; Brousse, T.; Lestriez, B.; Guyomard, D.; Gaubicher, J. *Energy Environ. Sci.* **2012**, *5*, 5379−5386.
(8) McCreery, R.; Dieringer, J.; Solak, A. O.; Snyder, B.; Nowak, A. M.; McGovern, W. R.; DuVall, S. *J. Am. Chem. Soc.* **2003**, *125*, 10748−10758.
(9) Combellas, C.; Delamar, M.; Kanoufi, F.; Pinson, J.; Podvorica, F. I. *Chem. Mater.* **2005**, *17*, 3968−3975.
(10) Schuster, D. I.; Megiatto, J. D. *Nat. Chem.* **2009**, *1*, 182−183.
(11) Gooding, J. *J. Electroanal.* **2008**, *20*, 573−582.
(12) Ehli, C.; Oelsner, C.; Guldi, D. M.; Mateo-Alonso, A.; Prato, M.; Schmidt, C.; Backes, C.; Hauke, F.; Hirsch, A. *Nat. Chem.* **2009**, *1*, 243−249.

(13) Barbier, B.; Pinson, J.; Desarmot, G.; Sanchez, M. *J. Electrochem. Soc.* **1990**, *137*, 1757−1764.
(14) Andrieux, C. P.; Gonzalez, F.; Savéant, J.-M. *J. Am. Chem. Soc.* **1997**, *119*, 4292−4300.
(15) Brooksby, P. A.; Downard, A. J.; Yu, S. S. C. *Langmuir* **2005**, *21*, 11304−11311.
(16) Nowall, W. B.; Wipf, D. O.; Kuhr, W. G. *Anal. Chem.* **1998**, *70*, 2601−2606.
(17) Malmos, K.; Iruthayaraj, J.; Pedersen, S. U.; Daasbjerg, K. *J. Am. Chem. Soc.* **2009**, *131*, 13926−13927.
(18) Zhang, L.; Sun, Y.; Lin, X. *Analyst* **2001**, *126*, 1760−1763.
(19) Vase, K. H.; Holm, A. H.; Norrman, K.; Pedersen, S. U.; Daasbjerg, K. *Langmuir* **2007**, *23*, 3786−3793.
(20) Allongue, P.; Delamar, M.; Desbat, B.; Fagebaume, O.; Hitmi, R.; Pinson, J.; Savéant, J.-M. *J. Am. Chem. Soc.* **1997**, *119*, 201−207.
(21) Yu, S. S. C.; Downard, A. J. *Langmuir* **2007**, *23*, 4662−4668.
(22) Brooks, S. A.; Dontha, N.; Davis, C. B.; Stuart, J. K.; O'Neill, G.; Kuhr, W. G. *Anal. Chem.* **2000**, *72*, 3253−3259.
(23) Bélanger, D.; Pinson, J. *Chem. Soc. Rev.* **2011**, *40*, 3995−4048.
(24) Barrière, F.; Downard, A. J. *J. Solid State Electrochem.* **2008**, *12*, 1231−1244.
(25) Pinson, J.; Podvorica, F. *Chem Soc. Rev.* **2005**, *34*, 429−439.
(26) Adenier, A.; Cabet-Deliry, E.; Chaussé, A.; Griveau, S.; Mercier, F.; Pinson, J.; Vautrin-Ul, C. *Chem. Mater.* **2005**, *17*, 491−501.
(27) Adenier, A.; Barré, N.; Cabet-Deliry, E.; Chaussé, A.; Griveau, S.; Mercier, F.; Pinson, J.; Vautrin-Ul, C. *Surf. Sci.* **2006**, *600*, 4801−4812.
(28) Tanguy, F.; Gaubicher, J.; Gaillot, A.-C.; Guyomard, D.; Pinson, J. *J. Mater. Chem.* **2009**, *19*, 4771−4777.
(29) Merson, A.; Dittrich, T.; Zidon, Y.; Rappich, J.; Shapira, Y. *Appl. Phys. Lett.* **2004**, *85*, 1075−1076.
(30) Maldonado, S.; Smith, T. J.; Williams, R. D.; Morin, S.; Barton, E.; Stevenson, K. J. *Langmuir* **2006**, *22*, 2884−2891.
(31) Belmont, J. A. U.S. Patent 5,554,739 (to Cabot Corp), 1996.
(32) Abiman, P.; Wildgoose, G. G.; Compton, R. G. *Int. J. Electrochem. Sci.* **2008**, *3*, 104−117.
(33) Abiman, P.; Wildgoose, G. G.; Compton, R. G. *J. Phys. Org. Chem,* **2008**, *21*, 433−439.
(34) Mesnage, A.; Lefèvre, X.; Jégou, P.; Deniau, G.; Palacin, S. *Langmuir* **2012**, *28*, 11767−11778.
(35) Lehr, J.; Williamson, B. E.; Downard, A. J. *J. Phys. Chem. C* **2011**, *115*, 6629−6634.
(36) Liu, Y. C.; McCreery, R. L. *J. Am. Chem. Soc.* **1995**, *117*, 11254−11259.
(37) Smith, R. D.L.; Pickup, P. G *Electrochim. Acta* **2009**, *54*, 2305−2311.
(38) Lebègue, E.; Madec, L.; Brousse, T.; Gaubicher, J.; Levillain, E.; Cougnon, C. *J. Mater. Chem.* **2011**, *21*, 12221−12223.
(39) Kalinathan, K.; Desroches, D. P.; Liu, X.; Pickup, P. G. *J. Power Sources* **2008**, *181*, 182−185.
(40) Smith, R. D.L.; Pickup, P. G. *Electrochem. Commun.* **2009**, *11*, 10−13.
(41) Pognon, G.; Brousse, T.; Demarconnay, L.; Bélanger, D. *J. Power Sources* **2011**, *196*, 4117−4122.
(42) Pognon, G.; Brousse, T.; Bélanger, D. *Carbon* **2011**, *49*, 1340−1348.
(43) Algharaibeh, Z.; Pickup, P. G. *Electrochem. Commun.* **2011**, *13*, 147−149.
(44) Algharaibeh, Z.; Liu, X.; Pickup, P G. *J. Power Sources* **2009**, *187*, 640−643.
(45) Padhi, A. K.; Nanjundaswamy, K. S.; Goodenough, J. B. *J. Electrochem. Soc.* **1997**, *144*, 1188−1194.
(46) Armand, M. Patent WO2002027823, 2001
(47) Gibot, P.; Casas-Cabanas, M.; Laffont, L.; Levasseur, S.; Carlach, P.; Hamelet, S.; Tarascon, J.-M.; Masquelier, C. *Nat. Mater.* **2008**, *7*, 741.
(48) William, R.; Evrard, D.; Gros, P. *J. Electroanal. Chem.* **2012**, *685*, 109−115.
(49) Wizansky, A. R.; Rauch, P. E.; Disalvo, F. J. *J. Solid State Chem.* **1989**, *81*, 203.
(50) Yamada, A.; Koizumi, H.; Nishimura, S. I.; Sonoyama, N.; Kanno, R.; Yonemura, M.; Nakamura, T.; Kobayashi, Y. *Nat. Mater.* **2006**, *5*, 357−360.
(51) Rodriguez-Carvajal, J. *IUCr-CPD Newsletter* **2001**, *26*, 12.
(52) Roisnel, T.; Rodríguez-Carvajal, J. In *Proceedings of the Seventh European Powder Diffraction Conference* (Barcelona, Spain); Delhez, R.; Mittenmeijer, E. J., Eds.; Trans Tech Publication: Switzerland, 2000, 118−123.
(53) Brunetti, G.; Robert, D.; Bayle-Guillemaud, P.; Rouvière, J. R.; Rauch, E. F.; Martin, J. F.; Colin, J. F.; Bertin, F.; Cayron, C. *Chem. Mater.* **2011**, *23*, 4515−4524.
(54) Nyquist, R. A. Interpreting Infrared, *Raman and Nuclear Magnetic Spectra*; Academic Press: New York, 2001; Vol. 2, p 173.
(55) Moreau, P.; Mauchamp, V.; Pailloux, F.; Boucher, F. *Appl. Phys. Lett.* **2009**, *94*, 123111−123113.
(56) Pazo-Llorente, R.; Bravo-Diaz, C.; Gonzalez-Romero, E. *Eur. J. Org. Chem.* **2004**, *15*, 3221−3226.
(57) Andrieux, C. P.; Pinson, J. *J. Am. Chem. Soc.* **2003**, *125*, 14801−14806.
(58) Delmas, C.; Maccario, M.; Croguennec, L.; Le Cras, F.; Weill, F. *Nat. Mater.* **2008**, *20*, 665−671.
(59) Seid, K. A.; Badot, J.-C.; Dubrunfaut, O.; Levasseur, S.; Guyomard, D.; Lestriez, B. *J. Mater. Chem.* **2012**, *22*, 2641−2649.
(60) Zhang, W.-J. *J. Power Sources* **2011**, *196*, 2962−2970.
(61) Leriche, J. B.; Hamelet, S.; Shu, J.; Morcrette, M.; Masquelier, C.; Ouvrard, G.; Zerrouki, M.; Soudan, P.; Belin, S.; Elkaim, E.; Baudelet, F. *J. Electrochem. Soc.* **2010**, *157*, A606−A610.
(62) Ouvrard, G.; Zerrouki, M.; Soudan, P.; Lestriez, B.; Masquelier, C.; Morcrette, M.; Hamelet, S.; Belin, S.; Flank, A. M.; Baudelet, F. *J. Power Sources* **2013**, *229*, 16−21.